Multi-conductor Line Models for Harmonic Load-flow Calculations in LV Networks with High Penetration of PV Generation

Fernando M. Camilo, M. E. Almeida, Rui Castro, and V. Fernão Pires

***Abstract*—Low-voltage (LV) distribution networks are unbalanced and present loads with nonlinear behavior, which introduce harmonics in the networks. The predictable increase in photovoltaic microgeneration (PV μG) accentuates this unbalanced characteristic, as well as poses new technical problems, namely voltage rise and reverse power flow. To accurately account for the distributed PV and loads in the LV network, unbalanced three-phase power flow algorithms should be utilized, where different approaches may be used to represent lines with various degrees of accuracy. The more accurate algorithm considers the electromagnetic coupling between the line conductors, whereas the simpler algorithm represents each conductor of the line as a single-phase line with pure resistive behavior. This paper aims to analyze the influence of the line model on the load flow in a highly unbalanced LV network with a high penetration of PV production, and considers the impact of the harmonics produced by nonlinear loads. Based on the results obtained, it is possible to identify the most suitable model to be used, depending on the study to be performed. Different scenarios of PV generation and loads are addressed in this paper.**

***Index Terms*—Line model, nonlinear loads, photovoltaic microgeneration, unbalanced distribution network.**

I. Introduction

RECENTLY, photovoltaic microgeneration (PV μG) located near end-user low-voltage (LV) consumers has increased significantly. The massive integration of PV μG near the prosumers (end-users that are simultaneously producers and consumers) poses new technical problems for the LV distribution networks, namely voltage rise and reverse power flow.

To accurately account for the distributed PV in the LV network, an unbalanced three-phase power flow analysis has gained significant attention from both academia and electrical utilities [1]. Numerous unbalanced three-phase load-flow methods neglect the mutual coupling between phases to simplify the algorithm and save considerable computational efforts. However, this simplification can yield inaccurate results for certain applications.

Therefore, the unbalanced three-phase load flow in LV distribution networks has recently been strongly addressed in literature. Reference [2] proposes an efficient real-imaginary decomposition-based method for a three-phase distribution power flow analysis of weakly meshed systems, which introduces a variation in the common backward-forward sweep (BFS) algorithm. A sequential power flow analysis method using a BFS algorithm for single-phase laterals and a sequence-component frame solver for three-phase networks are assessed in another study [3]. A three-phase power flow approach for distribution networks is proposed to preserve the original three-wire and four-wire configurations for a more accurate estimation of the impacts on different phases, neutrals, and grounding effects [4]. A complex vector-based model in a stationary reference frame $\alpha\beta 0$ has been developed to represent the power flow equations using a compact matrix and can be assessed in [5]. The authors claim that the use of an orthogonal reference frame simplifies the modeling of the distribution network component formulation. The use of smart electric vehicle (EV) charging and PV production to balance a three-phase four-wire distribution grid is addressed in [6]. This is achieved by controlling the EV chargers and PV inverters to transfer power from highly loaded to less loaded phases. Another study [7] considers PV nodes in active distribution networks and proposes an efficient method for handling PV nodes based on a loop analysis incorporated in the forward-backward sweep (FBS) algorithm framework. A complex affine arithmetic-based unbalanced three-phase FBS power flow method has been proposed to manage the uncertainties of solar and wind distributed generation (DG) [8]. A generalized admittance matrix approach in the Fortescue coordinate system has been proposed to solve unbalanced distribution networks [9]. A faster and more efficient load-flow technique for an unbalanced distribution system is also proposed [10], which is faster than others because it calculates the bus voltages in a single step, unlike the conventional BFS approach, which involves two separate

Manuscript received: October 15, 2020; revised: February 20, 2021; accepted: June 10, 2021. Date of CrossCheck: June 10, 2021. Date of online publication: July 27, 2021.

This work was supported by national funds through Fundação para a Ciência e a Tecnologia (FCT) (No. UIDB/50021/2020).

F. M. Camilo, M. E. Almeida, R. Castro (corresponding author), and V. Fernão Pires are with Instituto de Engenharia de Sistemas e Computadores, Investigação e Desenvolvimento (INESC-ID) and Técnico, University of Lisbon, Lisbon, Portugal, and V. Fernão Pires is also with ESTSetúbal, Polytechnics of Setúbal, Setúbal, Portugal (e-mail: fernando. camilo@tecnico. ulisboa. pt; d2527@tecnico.ulisboa.pt; rcastro@tecnico.ulisboa.pt; vitor.pires@estsetubal.ips.pt).

DOI: 10.35833/MPCE.2020.000740

steps. Another study [11] proposes a novel load-flow method for networks with multipoint-grounded-neutral and phase-to-neutral-connected equipment. The proposed load-flow, which is simple to implement, is a novel alternative calculation method that enables a fast and accurate load-flow calculation for unbalanced networks.

Consequently, it is important to know the parameters of self and mutual impedances for more accurate computations through robust power flow algorithms [1]. The mutual coupling effect can become substantial under the conditions of unbalanced phase loads or in the presence of harmonics caused by nonlinear loads. An aforementioned study [1] assesses the mutual coupling effect between medium-voltage (MV) and LV distribution lines, which share the same poles and power line corridor. The differences between the series impedance provided by the manufacturers are also compared with those calculated based on analytic methods [12]. A comparison between different approximation methods to model distribution lines for an unbalanced power flow is presented in another study [13]. All these studies indicate that to address unbalanced networks, the harmonic impact, among other issues, requires detailed line longitudinal and transversal parameters (data available from manufacturers are insufficient), considering the coupling in the multi-conductor line equations.

This paper intends to contribute to the discussion by performing a thorough investigation using several line models with different levels of accuracy and comparing the unbalanced three-phase load-flow bus voltages and power loss results. The reference case is the detailed line model, which is characterized by the full 4×4 impedance and admittance matrices. The investigation includes a study of the fundamental frequency and a harmonic study in which the loads are nonlinear.

The novelty of this paper is that it quantifies the voltage and power loss deviations associated with the use of simpler line models against the use of a full detailed line model in highly-unbalanced LV networks with a high share of PV generation, and considers different levels of harmonic contents originating from residential loads.

Overall, the major contribution of this paper is that the validity conditions of using simpler models to characterize the distribution lines (overhead lines and underground cables) are defined in unbalanced three-phase load flow studies, whether performed at a fundamental frequency or considering harmonic contents.

The remainder of this paper is organized as follows. Section II presents the proposed methodology and models used in the investigation. Section III defines the case study for analysis, whereas the results are presented in Section IV and discussed in Section V. Section VI draws the main conclusions of this paper.

II. Method Formulation

This section presents a three-phase load-flow algorithm that is able to analyze unbalanced LV radial distribution networks with a high penetration of PV generation. The developed formulation allows the use of models with different degrees of complexity to represent the line segments (overhead line or underground cable). This flexibility of the proposed model is important, as it makes it possible to compare the performance of the different models used to represent the line, allowing the most suitable selection for each application.

Certain changes have been made to the initial algorithm previously used in [14] to characterize the effect of nonlinear loads on LV distribution networks. These changes are related and characterize the rising impact of harmonics on the LV network due to nonlinear loads.

A. Three-phase Load Flow Algorithm

The method described in this paper is used for the load-flow calculation in an unbalanced LV network based on the BFS algorithm, where the solution techniques may be classified as the current summation method [15], [16], power summation method [14], [17], and admittance summation method [18]. There are several powerful load-flow methods existing in scientific literature such as the Newton-Raphson method, which is a load-flow method usually used in transmission grids. However, methods such as Newton-Raphson present convergence problems if the R/X ratio is high, as is the case with LV distribution networks. Furthermore, the Newton-Raphson method may not converge in radial networks, as proven in [19], where the effectiveness of the BFS method is compared with the traditional Gauss-Seidel and Newton-Raphson methods. On the other hand, the BFS algorithm has a better performance than the Newton-Raphson method for radial networks, as proven in [20], and has a good convergence level for networks with a high R/X ratio, which is demonstrated in [20], [21]. The proposed algorithm follows the main steps of the algorithm described in [14]. Nevertheless, unlike the algorithm in [14], which is based on BFS using the power summation method [17], the algorithm proposed in this paper is based on the current summation method that is assessed in [22], [23], and supports automatic voltage regulation transformer features based on the model suggested in [24].

The algorithm proposed in [14] is chosen upon a comparison with other suitable algorithms because it maintains the 4×4 matrix structure, as previously indicated, thereby allowing the explicit calculation of phase and neutral quantities, which are significantly useful for unbalanced network assessments. Another advantage of this method is the possibility of defining the load characteristics through the well-known load elasticity concept, thereby allowing the testing of different types of loads.

The iterative method to solve the radial system consists of three main steps, as described below.

1) Step 1: Nodal Current Calculation

The first step of this method is to calculate all the nodal currents in the network, following the methodology described in [25], [26]. For instance, for bus m and iteration k, the nodal currents $\boldsymbol{I}_m^{(k)}$, which is defined as a 4×1 matrix, is obtained by:

$$\boldsymbol{I}_m^{(k)}=\left[\left(\frac{S_{Rm}^{(k-1)}}{V_{Rm}^{(k-1)}}\right)^* \quad \left(\frac{S_{Sm}^{(k-1)}}{V_{Sm}^{(k-1)}}\right)^* \quad \left(\frac{S_{Tm}^{(k-1)}}{V_{Tm}^{(k-1)}}\right)^* \quad I_{Nm}^{(k-1)}\right]^{\mathrm{T}}-\boldsymbol{Y}_{mn}\boldsymbol{V}_m^{(k-1)} \tag{1}$$

where $S_{jm}=S_{jm_{\mu G}}-S_{jm_{ld}}\ (j=R,\ S,\ T)$ is the injected power at each phase of bus m, $S_{jm_{\mu G}}$ is the complex power of PV μG, $S_{jm_{ld}}$ is the load power; the superscript * denotes the conjugate operator; $I_{Nm}^{(k-1)}$ is the injected neutral current of bus m; $\boldsymbol{Y}_{mn}$ is the 4×4 transversal admittance matrix; and $\boldsymbol{V}_m^{(k-1)}$ is a 4×1 matrix that contains the voltages of bus m.

A simple exponential model is used to represent the loads because it is one of the most frequently used models that represents static loads [27]. The loads are characterized by their elasticity, ε, with respect to the voltage, and at each iteration k, the load power should be calculated by:

$$S_{jm_{ld}}^{(k)}=S_{jm_{ld}}^{(k-1)}\left(\left|V_{jm}\right|^{(k-1)}\Big/V_{rated}\right)^{\varepsilon} \quad j=R,S,T \tag{2}$$

where V_{rated} is the rated voltage that is made equal to 1 p.u..

For the first iteration, a flat voltage profile equal to the root node voltage (slack bus voltage $\boldsymbol{V}_{ref}$) is assumed as $\boldsymbol{V}_m^{(0)}=\boldsymbol{V}_{ref}$.

2) Step 2: Backward Sweep

This step consists of the branch current calculation, starting with the most distant nodes of the source node and moving toward the root node. As a result, the current in the line section mn for iteration k can be expressed as:

$$\boldsymbol{J}_{mn}^{(k)}=-\boldsymbol{I}_n^{(k)}+\sum_{x\in X}\boldsymbol{J}_{nx}^{(k)} \tag{3}$$

where $\boldsymbol{J}_{mn}^{(k)}$ is a 4×1 matrix that contains the currents of the phases and the neutral flowing in line section mn; $\boldsymbol{I}_n^{(k)}$ is a 4×1 matrix that contains the nodal currents for bus n; X is the set of cable sections connected to node n; and $\boldsymbol{J}_{nx}^{(k)}$ is a 4×1 matrix similar to $\boldsymbol{J}_{mn}$, nonetheless containing the currents that flow in all other line sections connected to bus n.

3) Step 3: Forward Sweep

This step starts from the source node and moves further away from the node. As a result, the voltage at node n for iteration k can be expressed as:

$$\boldsymbol{V}_n^{(k)}=\boldsymbol{V}_m^{(k)}-\boldsymbol{Z}_{mn}\boldsymbol{J}_{mn}^{(k)} \tag{4}$$

where $\boldsymbol{V}_n$ and $\boldsymbol{V}_m$ are 4×1 matrices containing the voltages at bus n and m, respectively; and $\boldsymbol{Z}_{mn}$ is the 4×4 longitudinal impedance matrix. Following these steps, and for iteration k, the power injection differences at each node for all the phases and the neutral wire are calculated by:

$$\begin{cases}\Delta S_{jm}^{(k)}=V_{jm}^{(k)}\left(I_{jm}^{(k)}\right)^*-\sum\limits_{i=R,S,T,N}Y_{mn_{ji}}^*\left|V_{im}^{(k)}\right|^2-S_{jm}^{(k-1)}\\ \Delta S_{Nm}^{(k)}=V_{Nm}^{(k)}\left(I_{Nm}^{(k)}\right)^*-\sum\limits_{i=R,S,T,N}Y_{mn_{Ni}}^*\left|V_{im}^{(k)}\right|^2\end{cases} \tag{5}$$

where $\Delta S_{jm}^{(k)}$ and $\Delta S_{Nm}^{(k)}$ are the power injection differences for the phases and neutral, respectively; and $Y_{mn_{ji}}$ is the element of line j and column i of matrix $\boldsymbol{Y}_{mn}$ ($i,j=R,\ S,\ T,\ N$).

When the difference between two consecutive values is greater than a specified value of tolerance (10^{-10} in this algorithm), all procedures are repeated from *Step 1* to *Step 3* until convergence.

The algorithm proposed in this paper has a 4×4 matrix configuration; however, it is possible to easily adapt the algorithm to a 3×3 matrix configuration in the case of Kron's reduction. This algorithm has been tested, compared, and validated by recurring to the test feeders IEEE 13-bus and IEEE 37-bus radial distribution networks [15], [16]. The accuracy has been validated by comparing the relative deviations between the bus voltage profile computed by the proposed algorithm and the results presented in literature. A powerful and well-known software platform named OpenDSS (http://smartgrid.epri.com/SimulationTool.aspx), an electrical power distribution system simulator, is used to compare the simulation results for both the fundamental frequency and harmonic load flow. Furthermore, for the fundamental frequency load flow, our model is also compared with the radial distribution analysis package of WH Power Consultants, Las Cruces, New Mexico) and Windmil (developed by Milsoft Integrated Solutions, Abilene, Texas). The results are available in [15] and [16]. In all the tests performed, the relative deviations for the fundamental frequency are always less than 0.3% compared with [15], [16], and less than 1.4% when OpenDSS software is used. These results can be found in Appendix A Table AI. Therefore, the proposed algorithm has been validated and used in the following research studies and is applied to a real radial three-phase unbalanced LV distribution network with a high penetration of PV generation.

B. Three-phase Harmonic Load-flow Algorithm

The iterative method to solve the three-phase harmonic load-flow algorithm based on [28], [29] consists of four main steps as described below.

1) Step 1: Load-flow Solution at Fundamental Frequency

In the first step, results are obtained for the fundamental frequency using the load-flow algorithm, as indicated in Section II-A.

2) Step 2: Load Model

The second step is related to the load modeling. Nonlinear loads are the causes of harmonics in the LV network; thus, the load model used should be able to characterize this effect. The choice of the load models depends on the nature of the load, several of which have been proposed in literature (see [30], for instance). Electronic loads are active and nonlinear; therefore, the current injected into these loads is usually distorted. Thus, its behavior can be regarded as a current source. In this paper, a model based on this concept [30] is used. The load is represented by an equivalent circuit with an RL branch parallel to the current source $I(\omega)$. The non-sinusoidal periodic current i can be expressed by two distinct components under steady-state conditions:

$$i=i_1+i_h=\sqrt{2}\,I_1\sin\left(\omega t-\phi_1\right)+\sqrt{2}\sum_{h=2}^{n}I_h\sin\left(h\omega t-\phi_h\right) \tag{6}$$

where i_1 is the fundamental component of the current; i_h is the total harmonic components; h is the harmonic order; I_1 is the root mean square (RMS) of the current for the fundamental frequency; I_h is the RMS of the current for the harmonic frequency h; ω is the angular frequency; ϕ_1 is the angle for

the fundamental frequency; and ϕ_h is the angle for the harmonic frequency h.

The current source $I(\omega)$ can also be replaced by a set of current sources in parallel with different frequencies. For example, for the harmonic h (with frequency $f_h = hf_1$, where f_1 is the fundamental frequency), the current source is $I(\omega = \omega_h) = I_h = |I_1| K_h$, where K_h is a complex multiplier defined for the frequency being solved. The angle α_h of the multiplier is based on the Fourier equations [31]:

$$\alpha_h = \alpha_1 h + \phi_h \tag{7}$$

where α_1 is the angle of the current for the fundamental frequency; and ϕ_h is defined as the frequency being solved. The typical values $|K_h|$ and ϕ_h can be obtained from literature [32]-[35].

The values of R and L are calculated for the fundamental frequency f_1 ($\omega_1 = 2\pi f_1$) based on the complex power of the load S_{ld}, and the bus voltage to which the load is connected. For instance, for a load connected to phase j ($j = R, S, T$) of bus m characterized by $S_{jm_{ld}} = P_{jm_{ld}} + jQ_{jm_{ld}}$, the parameters $R_{jm_{ld}}$ and $L_{jm_{ld}}$ are given by:

$$\begin{cases} R_{jm_{ld}} = P_{jm_{ld}} \dfrac{|V_{jm}|^2}{P_{jm_{ld}}^2 + Q_{jm_{ld}}^2} \\ L_{jm_{ld}} = \dfrac{1}{\omega_1} Q_{jm_{ld}} \dfrac{|V_{jm_{ld}}|^2}{P_{jm_{ld}}^2 + Q_{jm_{ld}}^2} \end{cases} \tag{8}$$

3) Step 3: Initialization of Harmonic Voltages

In this step, the following assumptions are adopted in the algorithm: ① the harmonic voltage distortion is null at the slack bus; and ② the nodal harmonic currents are only due to nonlinear loads because the PV μG system is assumed to be capable of filtering all the harmonics using the inverter capabilities.

Regarding the PV μG system, it should be noted that the harmonics injected into the network increase in lower radiations. However, the current PV system integration requirements into the grid regarding harmonic content are becoming increasingly strict. This can be observed in the legislation made available by the UK (EREC G83 Stds.) and VDE-AR-N4105, in which they impose a total harmonic distortion (THD) for PV integration of less than 3% [36]. In this manner, PV systems are usually operated at a significantly high frequency to fulfill the legislation requirements, thereby granting a low current distortion, despite being used under low solar radiation. Using the new generation of power semiconductors such as SiC MOSFETs, it is possible to operate the power converter at frequencies of approximately 100 kHz in hard switching. Furthermore, different harmonic distortion standards are imposed to consider the requirements of the PV system integration into the grid such as IEEE 1547, AS 4777.2 (Australia), GB/T (China), ECM (Malaysia), and UK (EREC G83 Stds.) and IEC 61000-3-2. In all of these, the current THD is significantly strict, which explains why commercial PV systems present very low THD harmonics. For example, in field tests [37], it has been verified that the 5th-order harmonic is the greatest, whose values, however, are below the limit of 2%. The same conclusion is reached when consulting commercial PV system catalogs. On the other hand, it is also possible to use an active power filter associated with the PV system to ensure a low THD that the legislation requires. In light of these considerations, we simplify this part of the system by assuming that the PV system does not inject harmonics beyond the fundamental. Nevertheless, we have performed THD tests considering the LV distribution system with and without PV generation (the results of these tests are presented in Table VI in Section IV).

Considering index h as the harmonic frequency order, the backward sweep step is represented by:

$$\left(\boldsymbol{J}_{mn}\right)_h = -\left(\boldsymbol{I}_n\right)_h + \sum_{x \in X} \left(\boldsymbol{J}_{nx}\right)_h \tag{9}$$

However, they are now related to frequency f_h, and the elements of $\left(\boldsymbol{I}_n\right)_h$ are the currents injected by nonlinear loads. The branch current calculation starts with the most distant nodes of the source node and moves toward the root node.

The forward sweep is calculated by:

$$\left(\boldsymbol{V}_n\right)_h = \left(\boldsymbol{V}_m\right)_h - \left(\boldsymbol{Z}_{mn}\right)_h \left(\boldsymbol{J}_{mn}\right)_h \tag{10}$$

where the variables indicate the same meanings as presented in (4). However, they are now related to frequency f_h. The node voltage calculation starts from the source node and moves further away from the node. This step consists of only one backward sweep iteration followed by a forward sweep iteration. Similar to the current injection method [28], [38], the currents due to nonlinear loads are considered constant in the calculation process.

4) Step 4: Calculation of Harmonic Voltages

The final step is to calculate the node voltages for the harmonic h, considering that the current injection due to nonlinear loads remains constant throughout the calculation process. On the other hand, nonlinear loads are represented by a current source in parallel with an impedance, with the parameters R and L defined in (8). Therefore, at iteration k, the currents are calculated as:

$$\left(\boldsymbol{I}_m\right)_h^{(k)} = \left(\boldsymbol{I}_m\right)_h^{(k-1)} - \left(\boldsymbol{Y}_{mn} + \boldsymbol{Y}_{ld}\right)_h \left(\boldsymbol{V}_m\right)_h^{(k-1)} \tag{11}$$

where $\boldsymbol{Y}_{ld}$ is a 4×4 diagonal matrix, and the first three elements of the diagonal represent the total load admittances (inverse of the impedances) connected to phases R, S, and T, and the fourth element is zero.

Then, the backward sweep is applied as:

$$\left(\boldsymbol{J}_{mn}\right)_h^{(k)} = -\left(\boldsymbol{I}_n\right)_h^{(k)} + \sum_{x \in X} \left(\boldsymbol{J}_{nx}\right)_h^{(k)} \tag{12}$$

The forward sweep is calculated by:

$$\left(\boldsymbol{V}_n\right)_h^{(k)} = \left(\boldsymbol{V}_m\right)_h^{(k)} - \left(\boldsymbol{Z}_{mn}\right)_h \left(\boldsymbol{J}_{mn}\right)_h^{(k)} \tag{13}$$

Following these steps, the power injection differences at each node for all the phases and neutral wire are calculated iteratively, following the procedures described in Section II-A. When the difference between two consecutive values is greater than a specified value of tolerance (10^{-10} in this algorithm), all the procedures are repeated from *Step 1* to *Step 4* until convergence.

This algorithm has been tested, compared, and validated

recurring to [29], [39], [40]. The accuracy has been validated by comparing the weight of each harmonic from the spectrum (relation between the voltage magnitude for harmonic h with that obtained for the fundamental frequency) using the proposed algorithm and those presented in the aforementioned references. In all the tests performed, the relative deviations are less than 8% compared with [29], and less than 11% when OpenDSS software is used. These results are presented in Appendix A Table AII. Therefore, the proposed algorithm has been validated and used in the following studies and applied to a real radial three-phase unbalanced LV distribution network with a high penetration of PV generation considering harmonics.

As the harmonics are considered, the RMS value of the voltages in each bus is obtained by considering the RMS values of the voltages for each harmonic [41], [42].

III. Characterization of Studies Performed

This paper aims to study the influence of the line model on load-flow results for a typical unbalanced LV radial network with a high penetration of PV production, and considers the impact of harmonics produced by nonlinear loads. The line models analyzed present different degrees of accuracy. The more accurate model considers the coupling between the line conductors, where the line parameters are characterized by two 4×4 full matrices, the longitudinal impedance matrix, and the transversal admittance matrix. This approach is used in the algorithms proposed in Section II. The simpler line model neglects the inductive and capacitive effects of the line and considers the line to be perfectly symmetric and under balanced conditions. Consequently, each conductor of the line is represented as a single-phase line with pure resistive behavior.

In Section III-A, all the cases analyzed in this paper are identified. The different line models are presented, as well as the manner in which they are implemented in the algorithms proposed in Section II. The extremely unbalanced LV network with a high PV μG penetration used for the studies is presented in Section III-B, and the criteria used in selecting the simulation results are analyzed in Section III-C.

A. Identification of Cases Analyzed

The cases analyzed are divided into two groups, Group A and Group B. In Group A, all the residential loads are considered linear; therefore, the unbalanced LV test network is considered for the analysis at the fundamental frequency (50 Hz), and the algorithm described in Section II-A is used.

In Group B, the same unbalanced LV test network is used; however, now it is considered that all residential loads present nonlinear behavior. The harmonic load flow algorithm described in Section II-B is used to perform the studies in this group of simulations. To represent the harmonic spectrum originating from nonlinear loads, two different scenarios are considered. In the first scenario, the loads originate from a low harmonic distortion (Group B-1), and in the other scenario, the loads originate from a high harmonic distortion (Group B-2). The harmonic spectrum values for each scenario are estimated from the existing data accessed in [32], [43] and are presented in Table I (values used in Group B-1) and Table II (values used in Group B-2), respectively. The values presented are the order of the harmonic h, its weight $|K_h|$, and its angle ϕ_h. The parameters are defined in Section II-B.

TABLE I
Harmonic Spectrum for Low Distortion Scenario (Group B-1)

h	$\lvert K_h\rvert$ (%)	ϕ_h (°)	h	$\lvert K_h\rvert$ (%)	ϕ_h (°)	h	$\lvert K_h\rvert$ (%)	ϕ_h (°)
1	100	–19	11	16	117	21	9	273
3	72	335	13	16	307	23	7	255
5	44	337	15	14	286	25	7	272
7	30	39	17	11	278			
9	23	7	19	10	53			

TABLE II
Harmonic Spectrum for High Distortion Scenario (Group B-2)

h	$\lvert K_h\rvert$ (%)	ϕ_h (°)	h	$\lvert K_h\rvert$ (%)	ϕ_h (°)	h	$\lvert K_h\rvert$ (%)	ϕ_h (°)
1	100	–11	11	18	358	21	12	295
3	80	348	13	17	332	23	10	237
5	54	341	15	15	296	25	8	315
7	36	345	17	14	294			
9	25	351	19	13	301			

In each group, six cases are defined, concerning the line model used.

1) Case I is the base case in which a more accurate line model is used. The line parameters per unit length are characterized by two full 4×4 matrices $\boldsymbol{Z}$ and $\boldsymbol{Y}$.

2) Case II neglects the transversal parameters of the line. In this case, the line is characterized only by the longitudinal impedance matrix $\boldsymbol{Z}$. In the algorithms described in Section II, this case is characterized by imposing $\boldsymbol{Y}=\boldsymbol{0}$.

3) In Case III, the line is considered perfectly symmetric and under balanced conditions. Therefore, each conductor of the line is represented by the single-phase equivalent parameters. In the algorithms described in Section II, this case is characterized using $\boldsymbol{Z}=\boldsymbol{Z}_{eq}$ and $\boldsymbol{Y}=\boldsymbol{Y}_{eq}$, where $\boldsymbol{Z}_{eq}$ and $\boldsymbol{Y}_{eq}$ are diagonal matrices, and are the diagonal elements of the single-phase equivalent parameters.

4) In Case IV, the line is considered perfectly symmetric and under balanced conditions; however, the inductive and capacitive effects are neglected. In the algorithms described in Section II, this case is characterized using $\boldsymbol{Z}=\mathrm{Re}\{\boldsymbol{Z}_{eq}\}=\boldsymbol{R}_{eq}$ and $\boldsymbol{Y}=\boldsymbol{0}$.

5) In Case V, the line is considered perfectly symmetric and under balanced conditions; however, the capacitive effect is neglected. In the algorithms described in Section II, this case is characterized using $\boldsymbol{Z}=\boldsymbol{Z}_{eq}$ and $\boldsymbol{Y}=\boldsymbol{0}$; however, now the value of the resistive part of the impedance is based on manufacturer data obtained from reference [44] with a reactance value that is 10% of the resistance.

6) Case VI is analogous to Case IV, where $\boldsymbol{Z}=\boldsymbol{Z}_{eq}$ and $\boldsymbol{Y}=\boldsymbol{0}$; however, the resistive parameter now takes the value of Case V.

B. Unbalanced LV Distribution Test Network

The LV distribution test network used in this paper is based on a real radial LV distribution network in the southern part of Portugal. Data are kindly provided by the Energias de Portugal (EDP), the largest Portuguese utility. Figure 1 presents the single-line diagram of the radial LV distribution test network, with a total of 55 buses, 54 branches, and 154 residential consumers, of which 75 are prosumers. Each prosumer has a set of PV panels with a peak power of 1.5 kW. The distribution transformer is a 15 kV/400V-230 V, 630 kVA transformer with a connection of delta-star with neutral (Dyn). In Fig. 1, C represents consumers; P represents presummers; and B1-B54 are the branches of the network.

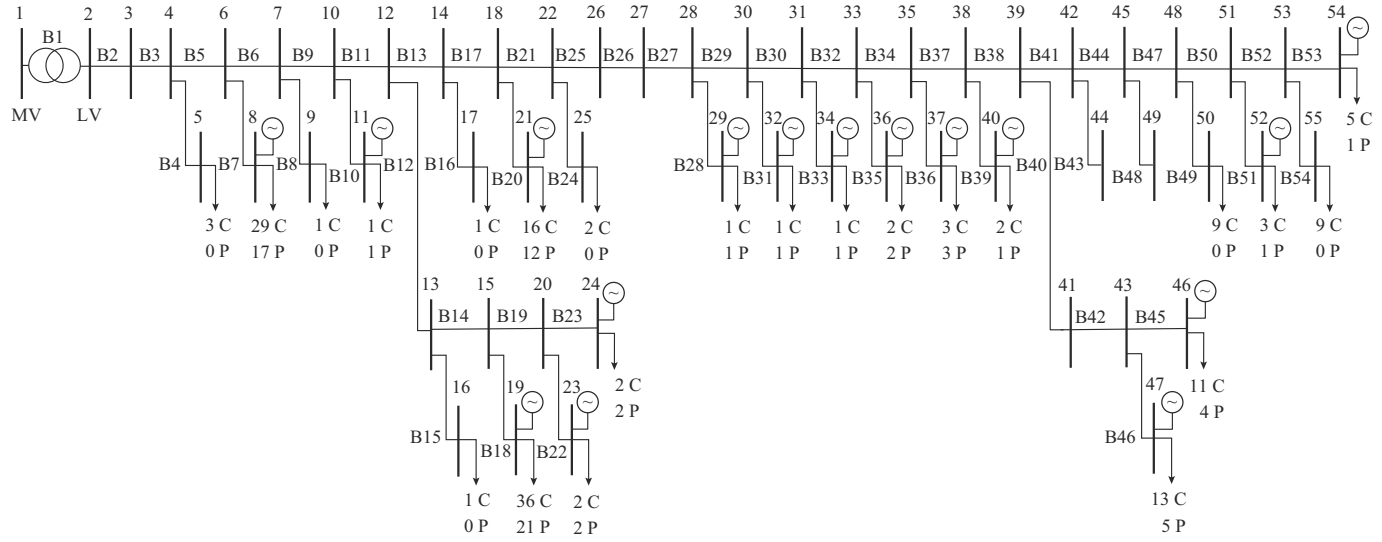

Fig. 1. Single-line diagram of radial LV distribution test network.

The distribution of the residential consumers and prosumers by each phase is as follows: 67 consumers of which 18 are prosumers in phase *R*, 44 consumers of which 24 are prosumers in phase *S*, and 43 consumers of which 33 are prosumers in phase *T*.

From the data made available by the Energy Services National Regulatory Authority (ERSE) [45], based on an average of 15-min intervals, a typical summer day at 02:00 p.m. presents the most severe conditions to the LV network (high PV generation and low consumption). All the consumption and generation data used in the simulations are listed in Appendix A Table AIII. Thus, the scenario used in the studies is constructed for this situation. Given the irradiance and temperature conditions at 02:00 p.m., the maximum output power that each PV μG is expected to achieve is approximately 1.15 kW (assuming the PV μG with a unitary power factor). The individual peak-load demand at 02:00 p.m. is approximately 0.50 kVA. Table III presents the total injected power of PV μG and the load power at 02:00 p.m. in phases *R*, *S*, and *T*.

TABLE III
TOTAL INJECTED POWER OF PV μG AND LOAD POWER AT 2:00 P.M. ON A TYPICAL SUMMER DAY

Phase	Injected power of PV μG (kVA)	Load power (kVA)
R	20.64	33.60
S	27.52	22.07
T	37.83	21.56
Total	85.99	77.23

At 02:00 p.m., the total PV power is 85.99 kVA, and the total load power is 77.23 kVA; thus, the PV penetration ratio is 111%. Regarding the entire day, the prosumers self-consume 45% of the total consumed energy, while the remaining 55% of electricity is consumed from the grid.

The studies are performed considering the branches of the LV test network (Fig. 1) composed only of underground cables or overhead lines. The ElectroMagnetic Transients Program/Alternative Transients Program (EMTP/ATP) is used to calculate the line parameters (underground cable or overhead line). Considering the test network constituted by the underground cables, the following two four-wire LSVAV cables are considered: 4×95 mm^2 and 4×16 mm^2. To obtain the single-phase equivalent parameters of the cables, which are used in Case III, the matrices are first transformed into being perfectly symmetric (calculating the average values of diagonal elements and the off-diagonal elements) and then the balanced condition is considered.

For the studies considering the test network constituted by the overhead lines, the four-wire lines considered are LXS: 4×95 mm^2 and 4×16 mm^2. In short, LXS cable means that the conductor is multi-strand aluminum with cross-linked polyethylene (PEX) insulation material. These four conductors are twisted; thus, the per-unit length parameters present only two different values: the self-coefficient and the mutual coefficient. The single-phase equivalent parameters of the lines, which are used in Case III, are obtained considering the balanced condition.

To perform the studies for Cases V and VI, the manufacturer data are used. The resistance value is obtained from reference [44], and the reactance value is considered to be 10%

of the resistance value. Equal values are used for the cable and line with the same cross-section.

C. Selection of Simulation Results to Be Analyzed

One of the problems associated with unbalanced LV networks with a high penetration of PV μG is related to the possibility that the voltage magnitude is not within the set limits. Therefore, it is important to analyze the influence of the line model on the network voltage profile. The results presented in Section IV show the maximum value of the voltage relative deviation, $\Delta V_{\max}(\%)$ for a selected bus of the network using the voltage obtained in Case I (of each group A or B) for the same bus as the reference value (base case value). The maximum value of the relative voltage deviation is given by:

$$\Delta V_{\max}(\%) = \max_{X \in \{RS, ST, TR\}} \left\{ \left(\left| V_X^{BC} \right| - \left| V_X \right| \right) \Big/ \left| V_X^{BC} \right| \right\} \times 100\% \quad (14)$$

where $\left|V_X^{BC}\right|$ (X=RS, ST, TR) represents the phase-to-phase magnitude voltage for Case I; and $|V_X|$ is the corresponding value obtained for one of the other cases (Cases II-VI).

The concept of voltage unbalance factor (VUF) is used to choose the set of nodes from the test network to be analyzed. International standards such as EN-50160 [46] or IEC 61000-3-x series, set a 2% limit of unbalanced voltage for LV networks. The level of voltage imbalance present in a system is defined in European standards such as VUF [47] and IEC 60034-26 [48]. Therefore, the degree of imbalance is defined by the relationship between the magnitudes of the negative sequence voltage $\left|V_{neg}\right|$ and positive sequence voltage $\left|V_{pos}\right|$, which is expressed as:

$$VUF = \frac{\left|V_{neg}\right|}{\left|V_{pos}\right|} \times 100\% = \sqrt{\frac{1 - \sqrt{3 - 6\beta}}{1 + \sqrt{3 - 6\beta}}} \times 100\% \quad (15)$$

where β is represented by the phase-to-phase voltages magnitudes.

$$\beta = \left(\left|V_{RS}\right|^4 + \left|V_{ST}\right|^4 + \left|V_{TR}\right|^4 \right) \Big/ \left(\left|V_{RS}\right|^2 + \left|V_{ST}\right|^2 + \left|V_{TR}\right|^2 \right)^2 \quad (16)$$

Following this concept, the sets of nodes that have been chosen for the analysis in this paper are the bigger values of VUF for the base case.

The influence of the line model on the value obtained for the network power losses is also an important outcome to be analyzed. In the test network used, power losses originate from line losses. The contribution to the losses of a line connected between nodes m and n is:

$$P_{l_{mn}} = \mathrm{Re}\left\{ \left(\boldsymbol{J}_{mn}^* \right)^{\mathrm{T}} \boldsymbol{Z}_{mn} \boldsymbol{J}_{mn} \right\} \quad (17)$$

The total power losses are obtained by summing the contributions of all lines. Therefore, the total power loss relative deviation, $\Delta P_{l_T}(\%)$, is defined using the power loss value obtained in Case I, $P_{l_T}^{BC}$, and the value obtained for one of the other cases P_{lT} (Cases II-VI).

$$\Delta P_{l_T}(\%) = \left[\left(P_{l_T}^{BC} - P_{l_T} \right) \Big/ P_{l_T}^{BC} \right] \times 100\% \quad (18)$$

IV. Results

In this section, the results demonstrate the influence of the line model on the load-flow values obtained, considering the values calculated in Case I as the reference.

Section IV-A presents the relevant values obtained in the base cases at 50 Hz for Case I/Group A, Case I/Group B-1 (low harmonic distortion), and Case I/Group B-2 (high harmonic distortion). Sections IV-B and IV-C are dedicated to Group A and Group B, respectively, presenting the relative deviations between the base case and other cases. Finally, Section IV-D presents the simulations performed to assess the THDs with and without PV systems.

We recall that the purpose of this paper is to evaluate the influence of several line models on the load-flow results of an unbalanced LV distribution grid with PV embedded generation. To isolate the influence of the line models, all the remaining characteristics are maintained constant (PV generation, demand, topology, etc.); thus, the results obtained are not contaminated.

A. Base Case Results (Case I)

Using the LV test network with linear loads and representing the line with the more accurate model (Group A, Case I), two simulations have been performed: one considering the network constituted only by underground cables, and the other using only overhead lines. For both simulations, the results obtained indicate that bus 47 presents bigger VUF values of 3.06% and 2.92% using only underground cables or overhead lines, respectively. Therefore, the simulation results presented in this paper are concerned with this node.

Table IV presents the phase-to-phase voltages obtained for Case I/Group A (loads with linear behavior), Case I/Group B-1 (nonlinear loads originating from low harmonic distortion), and Case I/Group B-2 (nonlinear loads originating from high harmonic distortion). The results obtained for the base case of all the scenarios indicate that the voltage magnitude values are within the set limits (0.9-1.1 p.u.).

TABLE IV
Phase-to-phase Voltage of Bus 47 for Groups A, B-1, and B-2 in Case I

Group	Line type	$\left\|V_{RS}\right\|$ (p.u.)	$\left\|V_{ST}\right\|$ (p.u.)	$\left\|V_{TR}\right\|$ (p.u.)
Group A	Cables	0.9835	1.0315	0.9890
	Lines	0.9767	1.0254	0.9908
Group B-1	Cables	1.0058	1.0510	1.0245
	Lines	0.9971	1.0349	1.0097
Group B-2	Cables	1.0157	1.0594	1.0405
	Lines	1.0065	1.0394	1.0181

The total power loss values obtained for Case I of Groups A, B-1, and B-2 are presented in Table V. The values obtained for Group A are significantly smaller than those obtained for both scenarios of Group B. As expected, the power losses increase with an increase in the harmonic content in the network.

TABLE V
TOTAL POWER LOSS FOR GROUPS A, B-1, B-2 IN CASES I

Line type	$P_{l_T}^{BC}$ (kW)		
	Group A	Group B-1	Group B-2
Underground cables	4.68	23.86	29.12
Overhead lines	4.71	23.62	28.81

B. Group A Set Cases Results

Figure 2(a) presents the maximum values of the voltage relative deviation obtained for all the cases (Cases II-VI) and for bus 47, considering the network only with underground cables or only with overhead lines.

Although the influence of the line model on the results is insignificant, as the deviations found are less than 2%, it is important to highlight and discuss the results obtained. The line model used in Case III, which is perhaps one of the most used models in the LV network studies, presents accurate results and is a good choice in terms of the cost-benefit ratio.

The results shown in Fig. 2(a) present deviations of less than 1.1% for the network only with the cables and 0.01% for the network only with the overhead lines. This difference occurs because the overhead line considered already has a perfectly symmetrical configuration (conductors twisted) being closer to the conditions required to obtain the one-phase equivalent parameters. The results presented in Fig. 2(a) for Cases IV and VI demonstrate that as far as the overhead lines are concerned, neglecting the inductive part of the longitudinal impedance results in the worst relative deviations (up to 1.77%). Although the manufacturer data used to characterize the parameters of the cables and the overhead lines are the same, the results obtained in Cases V and VI are not equal (Fig. 2(a)). The differences occur because the base case values are not the same (see Table IV).

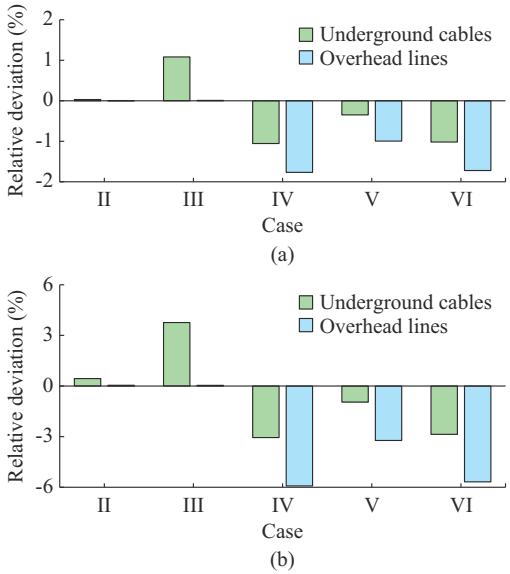

Fig. 2. The maximum values of voltage relative deviation for bus 47. (a) Group A results. (b) Group A results obtained by increasing 10 times the length of lines.

Based on the results obtained for Cases II, IV, V, and VI, it appears to be a valid option to neglect the transversal parameters of the line as the deviations found are less than 2%. However, to corroborate this conclusion, another study considering the same LV distribution network with higher line lengths has been conducted. Therefore, in this paper, the lengths of all lines are increased by 10 times (the average length of the lines, which is 36 m in the test network, is increased to 360 m). Figure 2(b) presents the obtained results.

Although all the deviation values increase, the model used in Case II remains valid, as the deviations found are less than 0.5%. Based on the results obtained, it is important to highlight that with the simpler model (Case IV) or using manufacturer data (Cases V and VI), the deviation values are negative and can reach near 6%. This indicates that the predicted voltage magnitude is greater than the actual voltage (that obtained with the base case model) and may exceed the voltage set limits, which does not occur in reality.

Figure 3 presents the power loss relative deviation for all the cases (Cases II-VI), considering the line lengths of the base case network and either with the underground cables or with the overhead lines. The deviations obtained are less than 4.2% and present a higher sensitivity to the line model used. Once again, Case II exhibits a lower deviation of less than 1%.

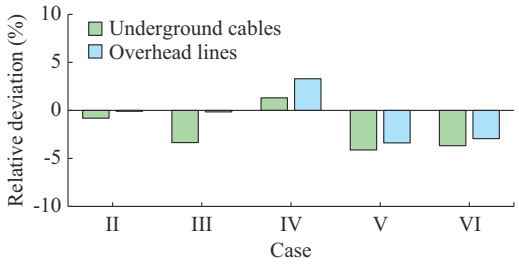

Fig. 3. Power losses relative deviation in Group A.

C. Group B Set Cases Results

Figures 4 and 5(a) present the maximum values of the voltage relative deviation obtained for Groups B-1 and B-2, respectively, for all cases (Cases II-VI) and for bus 47, considering the network with either the underground cables or overhead lines. We recall that in this group, the loads are assumed to have a nonlinear behavior; in Group B-1, they have a low harmonic distortion; while in Group B-2, they have a high harmonic distortion.

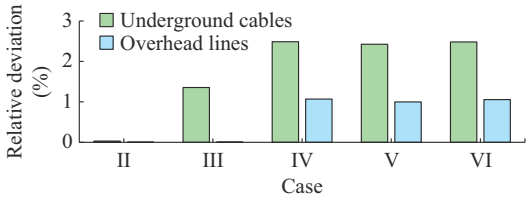

Fig. 4. The maximum values of voltage relative deviation in Group B-1 for bus 47.

The results presented in Fig. 4 and Fig. 5(a) compared with those obtained for Group A (Fig. 2(a)) present an in-

crease in the relative deviations as the harmonic content increases, except for Case II. Once again, the results in Case II demonstrate that it is valid to neglect the transversal parameters of the line, as the deviations found are less than 0.05%. When the LV network is analyzed considering the harmonic content, the reactive parameters (inductive and capacitive) of the line become more relevant. Therefore, the relative deviations obtained for Cases IV and VI (where only the resistive part is considered) present bigger values, which nearly reach 4% for the scenario of Group B-2.

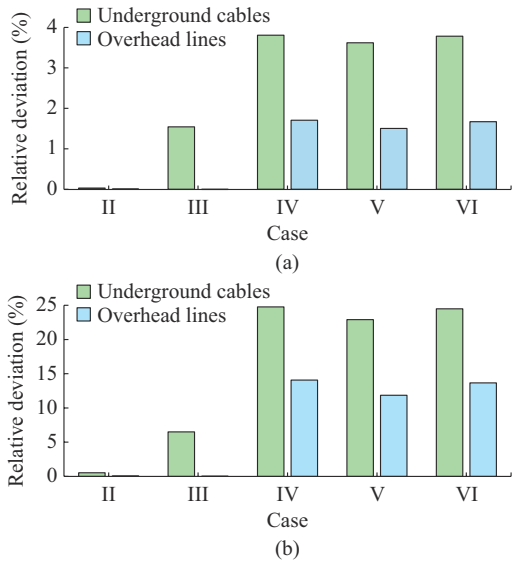

Fig. 5. The maximum values of the voltage relative for bus 47. (a) Group B-2 results. (b) Group B-2 results obtained by increasing 10 times the length of lines.

To draw more general conclusions regarding the influence of the line model used, it is important to study what happens if all line lengths are increased by 10 times (the average length of the lines, which is 36 m in the test network, is increased to 360 m). The results obtained for Group B-2 are presented in Fig. 5(b). The deviations increase significantly, particularly those concerning Cases IV-VI, reaching 24% for the scenario with a high harmonic content (Fig. 5(b)).

The results obtained for the power loss relative deviation for all the cases of Groups B-1 and B-2, respectively, considering the base case network either with the underground cables or with the overhead lines, indicate that for Cases II-IV, the power loss deviations are less than 0.7%. However, for Cases V and VI (which use manufacturer data), the deviations increase, reaching approximately 6%.

D. THD Simulations

The voltage THD is assessed considering the LV distribution network with and without the PV generators. The PV systems are considered to inject a 5th-order harmonic of 1.5% (which is typically more than what is presented in the catalogs) and 0.6% for the 7th-order harmonics. The results are presented in Table VI. Owing to space limitations, Table VI is shortened and displays only a small amount of the THD results for each node/phase of the grid. The worst case occurs at node 55 (in bold in Table VI).

The results present an impact on the THD, ranging from 31.2% without PVs to 32.8% with PVs, in the worst case (in bold). As far as the limits of the standards are concerned, we conclude that even before the introduction of the PV systems, the limits of the standards are not compliant owing to the nonlinear loads. When PV systems are introduced, we verify that the limits of the harmonic currents are obeyed; however, the impact of the voltage limits is limited. Regardless, this impact could be sufficient to not comply with the limits of the voltage THD defined by the standards in certain circumstances.

TABLE VI
VOLTAGE THD FOR EACH NODE/PHASE WITHOUT AND WITH PV GENERATORS

Node	THD without PV generators (%)			THD with PV generators (%)		
	Phase *R*	Phase *S*	Phase *T*	Phase *R*	Phase *S*	Phase *T*
1	0.0	0.0	0.0	0.0	0.0	0.0
2	0.0	0.0	0.0	0.0	0.0	0.0
3	8.4	8.5	6.4	9.2	9.1	7.4
4	12.8	12.9	9.8	13.9	13.6	11.0
5	12.9	12.9	9.8	14.0	13.6	11.0
6	14.9	15.1	11.4	16.1	15.7	12.7
7	16.6	16.8	12.7	17.9	17.4	14.1
8	15.1	15.3	11.5	16.3	15.9	12.8
9	16.6	16.8	12.7	17.9	17.4	14.1
10	18.3	18.5	14.0	19.7	19.1	15.4
11	18.4	18.5	14.1	19.7	19.1	15.5
⋮	⋮	⋮	⋮	⋮	⋮	⋮
55	**31.2**	28.4	21.0	**32.8**	28.7	22.4

This shows the importance of using accurate line models, as well as studying the influence of the transmission line model on load flow results, with a high penetration of PV generation and considering the impact of the harmonics produced by nonlinear loads.

V. DISCUSSION

Table VII summarizes the voltage deviations in relation to the base case (Case I) obtained for bus 47, where the values in bold represent those lower than 1%. We consider that the line models holding a maximum of 1% voltage deviation threshold represents the LV distribution network with an acceptable degree of accuracy.

The following conclusions may be drawn from Table VII, where ℓ represents the original length of the lines and 10ℓ represents that the lengths of the lines are increased by 10 times.

1) The line model characterized by Case II (longitudinal impedance matrix $\boldsymbol{Z}$ and imposing $\boldsymbol{Y}=\boldsymbol{0}$) is adequate to represent the LV distribution network in all the studied scenarios, as the voltage deviations obtained are always less than 1%.

2) Considering Case III (single-phase line equivalent parameters $\boldsymbol{Z}_{eq}$ and $\boldsymbol{Y}_{eq}$), it is adequate to represent the LV distribution network only if overhead lines are used, despite utiliz-

ing longer lengths or with nonlinear loads.

3) Regarding the line model of Case IV (single-phase line equivalent resistance to characterize the longitudinal impedance $\boldsymbol{Z}=\boldsymbol{R}_{eq}$ and imposing $\boldsymbol{Y}=\boldsymbol{0}$), it is not suitable to model the LV distribution network, either by using the lines or cables, as the deviations obtained are always greater than 1%.

4) The line model characterized by Case V (single-phase line equivalent longitudinal impedance using manufacturer data $\boldsymbol{Z}=\boldsymbol{R}_m(1+\mathrm{j}0.1)$ and imposing $\boldsymbol{Y}=\boldsymbol{0}$) is not satisfactory for modeling the LV distribution network using lines/cables if heavy nonlinear loads are present in the network or if the lines/cable lengths increase.

5) In terms of the line model defined by Case VI (single-phase line equivalent manufacturer resistance to characterize the longitudinal impedance $\boldsymbol{Z}=\boldsymbol{R}_m$ and impose $\boldsymbol{Y}=\boldsymbol{0}$), it is not acceptable to represent the LV distribution network using either lines or cables, as the voltage deviations obtained are high.

TABLE VII
VOLTAGE RELATIVE DEVIATIONS (RELATED TO CASE I) FOR BUS 47 AT 2:00 P.M.

Case	Length	Deviation of Group A (%)		Deviation of Group B-1 (%)		Deviation of Group B-2 (%)	
		Overhead lines	Underground cables	Overhead lines	Underground cables	Overhead lines	Underground cables
Case II ($\boldsymbol{Z}$, $\boldsymbol{Y}=\boldsymbol{0}$)	ℓ	**0.003**	**–0.03**	**0.003**	**0.03**	**0.003**	**0.030**
	10ℓ	**0.044**	**0.44**			**0.065**	**0.533**
Case III ($\boldsymbol{Z}_{eq}$, $\boldsymbol{Y}_{eq}$)	ℓ	**0.010**	1.08	**0.006**	1.36	**0.005**	1.540
	10ℓ	**0.040**	3.76			**0.027**	6.500
Case IV ($\boldsymbol{Z}=\boldsymbol{R}_{eq}$, $\boldsymbol{Y}=\boldsymbol{0}$)	ℓ	–1.770	–1.06	1.070	2.49	1.710	3.810
	10ℓ	–5.920	–3.06			14.100	24.800
Case V ($\boldsymbol{Z}=\boldsymbol{R}_m(1+\mathrm{j}0.1)$, $\boldsymbol{Y}=\boldsymbol{0}$)	ℓ	**–0.995**	**–0.35**	**0.999**	2.43	1.500	3.620
	10ℓ	–3.230	**–0.95**			11.860	22.900
Case VI ($\boldsymbol{Z}=\boldsymbol{R}_m$, $\boldsymbol{Y}=\boldsymbol{0}$)	ℓ	–1.720	–1.02	1.060	2.48	1.670	3.780
	10ℓ	–5.680	–2.86			13.700	24.500

A simulation has been performed at night (08:00 p.m.) to assess the impact of the load at its maximum and without PV generation. Table VIII summarizes the voltage deviations obtained for bus 47 at night (08:00 p.m.), where the values in bold represent those lower than 1%. In this simulation, the PV generation is zero and the load is at its maximum. The simulations are performed for Group A (linear loads, 50 Hz frequency) and Group B-2 (nonlinear loads, high harmonic distortion). Again, we consider that line models holding a maximum of 1% voltage deviation may be used to model the LV distribution network with an acceptable degree of accuracy.

TABLE VIII
VOLTAGE RELATIVE DEVIATION (RELATED TO CASE I) FOR BUS 47 AT 08:00 P.M.

Case	Length	Deviation of Group A (%)		Deviation of Group B-2 (%)	
		Overhead lines	Underground cables	Overhead lines	Underground cables
Case II ($\boldsymbol{Z}$, $\boldsymbol{Y}=\boldsymbol{0}$)	ℓ	**0.003**	**0.03**	**0.003**	**0.03**
	10ℓ	**0.042**	**0.43**	**0.058**	**0.40**
Case III ($\boldsymbol{Z}_{eq}$, $\boldsymbol{Y}_{eq}$)	ℓ	**0.060**	1.21	**0.046**	2.08
	10ℓ	**0.300**	4.85	**0.176**	9.38
Case IV ($\boldsymbol{Z}=\boldsymbol{R}_{eq}$, $\boldsymbol{Y}=\boldsymbol{0}$)	ℓ	–1.640	–1.93	1.820	4.21
	10ℓ	–6.600	–7.45	25.830	38.96
Case V ($\boldsymbol{Z}=\boldsymbol{R}_m(1+\mathrm{j}0.1)$, $\boldsymbol{Y}=\boldsymbol{0}$)	ℓ	**0.340**	**0.87**	2.320	4.56
	10ℓ	1.670	3.93	23.300	36.47
Case VI ($\boldsymbol{Z}=\boldsymbol{R}_m$, $\boldsymbol{Y}=\boldsymbol{0}$)	ℓ	**–0.780**	–1.22	2.520	4.76
	10ℓ	–2.060	–3.64	27.480	39.81

In general, the same conclusions drawn for the 02:00 p.m. scenario are applied for the 08:00 p.m. scenario. Here, we recall them for convenience. Line model II is accurate in all simulations; line model III can be used if overhead lines are considered. The loads may be considered as linear, and the LV distribution network is composed of short lines/cables. Line model V provides acceptable results, and the remaining line models lead to high voltage deviations in relation to the benchmark model (Case I). Therefore, they are not suited to perform power flow studies in LV distribution networks.

We have noticed an increasing trend in the voltage deviations registered for bus 47 at 08:00 p.m. compared with the previous daylight scenario owing to the simulated peak load situation. For instance, using the Case VI line model (longitudinal impedance equal to single-phase line equivalent manufacturer resistance) with heavy distorted loads, the line length is equal to 10 times the original line length, and the voltage deviation is 39.81% in the night scenario and 24.5%

in the 02:00 p.m. scenario. In both situations, the use of this model is unacceptable; however, the obtained voltage deviations are worse at 08:00 p.m.

VI. Conclusion

The operation of LV distribution networks is changing mainly owing to the increasing penetration of PV μG located near end-users. The most critical situation is by lunchtime when the PV is produced at a maximum and the consumption is low. Thus, the voltage profile is likely to rise, eventually reaching values higher than the maximum that is stipulated by the network operator to be safe for the system operation. This problem is aggravated when the harmonics introduced by nonlinear loads, which increasingly compose the LV consumer loads, are considered. In this context, there has been renewed interest in the power flow solution for LV distribution networks. These networks are inherently unbalanced, and the introduction of unbalanced PV generation is likely to increase the imbalance. Therefore, unbalanced three-phase power flow algorithms must be used to address this problem. A line model is a key input. The common practice in literature is to use simplified models, for instance, considering single-phase equivalent parameters, or manufacturer data, which are based on single-phase equivalent parameters. In addition, harmonics are typically not considered in the analysis.

In this paper, we analyze the influence of the line model on the power flow results of an LV network with a high penetration of PV μG. The line models used in this paper present different degrees of accuracy. The more accurate model considers the electromagnetic coupling between the line conductors, whereas the simpler model represents each conductor of the line as a single-phase line with pure resistive behavior. In addition, we analyze the impact of harmonics produced by nonlinear loads. The study has been performed considering the following two scenarios: one in which the loads originate low harmonic distortion, and the other where the loads originate high harmonic distortion. We quantify the voltage and power loss deviations of using the different line models in relation to the base case, in which a full detailed line model is used. When all residential loads present a linear behavior, we find that simple models can be used if the distances involved are modest (in our test networks, the average line length is 36 m). In this case, deviations lower than 2% are obtained. However, these figures easily increase when the distance is longer. For instance, when the average line length is 10 times higher, the simpler models can present deviations as high as 6% with respect to the full detailed line model.

When the harmonics are considered, the deviations increase and reach 4% in the scenario with a high harmonic content. However, when the average line length is 10 times higher, the deviations can exceed 24% in the scenario with a high harmonic content. THD assessment tests are performed considering the LV distribution network with and without PV generators. The harmonics injection by the PV system is concluded to be insignificant.

We have also studied a case in which there is no PV generation and the loads are at their maximum, portraying a night situation (08:00 p.m.). In general, the same conclusions drawn for the 02:00 p.m. scenario are applicable for the 08:00 p.m. scenario. However, we notice an increasing trend in the voltage deviations at 08:00 p.m. compared with the 02:00 p.m. case. For instance, using a line model with a longitudinal impedance equal to the single-phase line equivalent manufacturer resistance with heavy distorted loads and the line length equal to 10 times the original line length, the voltage deviation is 39.81% in the night scenario and 24.5% in the 02:00 p.m. scenario. All voltage deviations are measured against the base case model, in which a more accurate line model is used (two full 4×4 matrices $\boldsymbol{Z}$ and $\boldsymbol{Y}$).

This high deviation can be crucial in detecting whether a voltage is within or outside the secure boundaries defined by the network operator. For instance, using a simplified line model, a voltage can be predicted as being within the boundaries when in reality, the voltage is above the maximum limit when using accurate line models. In addition, an opposite situation can occur. This strongly recommends using full 4×4 impedance matrix detailed models (transversal parameters cannot be neglected) in long LV distribution networks with a high harmonic content.

Appendix A

A. Results Validation

To validate the three-phase load-flow algorithm described in Section II-A, IEEE 13-bus and IEEE 37-bus test feeders are used (network data obtained from https://site.ieee.org/pes-test-feeders/resources/). The results of the proposed algorithm are compared with those obtained using the OpenDSS software and with those presented in [15], [16]. As referred in [16], the results published are obtained using the following software: Radial Distribution Analysis Package (RDAP) of WH Power Consultants, Las Cruces, New Mexico, USA, and Windmil developed by Milsoft Integrated Solutions, Abilene, Texas, USA. Owing to space constraints, we only present the results using the IEEE 13-bus test feeder in Table AI. The values presented are per unit phase to the neutral bus voltages V_{iN} ($i=R, S, T$).

The proposed algorithm demonstrates a good performance and accuracy as the relative deviations obtained are less than 0.3% compared with [15], [16] and less than 1.4% when OpenDSS software is used.

The test network presented in [29] is used to validate the three-phase harmonic load-flow algorithm described in Section II-B. The results are compared with those obtained using the OpenDSS software and with those published in [29], which uses a BFS algorithm. Table AII presents the values obtained for harmonics 1 (fundamental), 3, and 5 related to V_{RN}, which is the phase-to-neutral voltage of phase R.

To compare the three methodologies, the relative deviations related to the weight of each harmonic are used. The weight of each harmonic is the ratio between the voltage magnitude for the harmonic h ($h=3, 5$) and the voltage magnitude for the fundamental frequency. The proposed algorithm presents a good performance and accuracy as the relative deviations obtained are less than 8% compared with [29] and less than 11% when OpenDSS software is used.

TABLE AI
RESULT COMPARISON OF IEEE 13-BUS TEST FEEDER

Node	References [15] and [16]			Proposed algorithm			OpenDSS		
	V_{RN} (p.u.)	V_{SN} (p.u.)	V_{TN} (p.u.)	V_{RN} (p.u.)	V_{SN} (p.u.)	V_{TN} (p.u.)	V_{RN} (p.u.)	V_{SN} (p.u.)	V_{TN} (p.u.)
611			0.9738			0.9745			0.9608
632	1.0210	1.0420	1.0174	1.0210	1.0420	1.0174	1.0143	1.0289	1.0042
633	1.0180	1.0401	1.0148	1.0181	1.0401	1.0148	1.0113	1.0270	1.0015
645		1.0329	1.0155		1.0328	1.0154		1.0197	1.0023
646		1.0311	1.0134		1.0311	1.0134		1.0180	1.0002
650	1.0000	1.0000	1.0000	1.0000	1.0000	1.0000	0.9999	1.0000	0.9999
652	0.9825			0.9797			0.9753		
671	0.9900	1.0529	0.9778	0.9871	1.0524	0.9784	0.9828	1.0403	0.9649
675	0.9835	1.0553	0.9758	0.9808	1.0546	0.9764	0.9763	1.0426	0.9629
680	0.9900	1.0529	0.9778	0.9870	1.0524	0.9784	0.9828	1.0403	0.9649
684	0.9881		0.9758	0.9855		0.9764	0.9809		0.9628

TABLE AII
V_{RN} FOR HARMONICS 1, 3, AND 5 IN [29], OBTAINED WITH PROPOSED ALGORITHM AND OPENDSS SOFTWARE

Node	V_{RN} for harmonic 1 (V)			V_{RN} for harmonic 3 (V)			V_{RN} for harmonic 5 (V)		
	Reference [29]	Proposed algorithm	OpenDSS	Reference [29]	Proposed algorithm	OpenDSS	Reference [29]	Proposed algorithm	OpenDSS
632	4082	4085	4078	31.763	30.361	30.202	39.813	37.423	38.662
633	4078	4078	4073	31.917	32.392	31.478	40.379	39.907	40.239
634	4077	4076	4072	31.945	32.834	31.713	40.485	40.452	40.527
645	4071	4064	4065	37.094	36.106	33.826	45.667	44.453	43.269
646	4066	4054	4058	37.229	38.545	35.207	46.189	47.405	45.014
650	4160	4160	4160	0.000	0.000	0.000	0.000	0.000	0.000
671	4034	4037	4016	44.517	44.119	47.152	57.365	54.254	60.326
680	4027	4023	4007	50.452	47.603	49.059	63.003	58.443	62.636

B. Consumption and Generation Data

Table AIII presents the consumption and generation data for a typical summer day of the year, which are available by the Energy Services National Regulatory Authority (ERSE) of Portugal [45].

TABLE AIII
CONSUMPTION AND GENERATION DATA FOR A TYPICAL SUMMER DAY OF YEAR

Time	Consumption (kW)	Generation (kW)	Time	Consumption (kW)	Generation (kW)
01:00	0.3520	0.0000	13:00	0.5124	1.1200
02:00	0.3096	0.0000	14:00	0.5016	1.1464
03:00	0.2916	0.0000	15:00	0.5080	1.1140
04:00	0.2844	0.0000	16:00	0.5252	1.0188
05:00	0.2880	0.0000	17:00	0.5372	0.8496
06:00	0.2992	0.0000	18:00	0.5680	0.6136
07:00	0.3080	0.0252	19:00	0.5940	0.3320
08:00	0.3584	0.1568	20:00	0.5816	0.1036
09:00	0.4184	0.3964	21:00	0.5488	0.0076
10:00	0.4656	0.6624	22:00	0.5256	0.0000
11:00	0.4872	0.8888	23:00	0.4860	0.0000
12:00	0.5108	1.0432	24:00	0.4228	0.0000

The data available present the proportion of annual energy consumption (for an LV consumer) or annual energy generation (for a PV generator) that is assigned to every 15 min of each day of the year. The values presented are obtained by calculating the correspondent power for every 15 min of a typical summer day. Due to space limitations, only hourly values are shown.

REFERENCES

[1] R. Yan and T. K. Saha, "Analysis of unbalanced distribution lines with mutual coupling across different voltage levels and the corresponding impact on network voltage," *IET Generation, Transmission & Distribution*, vol. 9, no. 13, pp. 1727-1737, Oct. 2015.

[2] G. Chang, S. Y. Chu, M. F. Hsu *et al*., "An efficient power flow algorithm for weakly meshed distribution systems," *Electric Power Systems Research*, vol. 84, no.1, pp. 90-99, Mar. 2012.

[3] M. Z. Kamh and R. Iravani, "Steady-state model and power-flow analysis of single-phase electronically coupled distributed energy resources," *IEEE Transactions on Power Delivery*, vol. 27, no. 1, pp. 131-139, Jan. 2012.

[4] M. J. E. Alam, K. M. Muttaqi, D. Sutanto *et al*., "Performance analysis of distribution networks under high penetration of solar PV," in *Proceedings of 44th International Conference on Large High Voltage Electric Systems*, Paris, France, Jan. 2012, pp. 1-9.

[5] P. Arboleya, C. Gonzalez-Moran, and M. Coto, "Unbalanced power flow in distribution systems with embedded transformers using the complex theory in $\alpha\beta 0$ stationary reference frame," *IEEE Transactions on Power Systems*, vol. 29, no. 3, pp. 1012-1022, May 2014.

[6] S. Weckx and J. Driesen, "Load balancing with EV chargers and PV

inverters in unbalanced distribution grids," *IEEE Transactions on Sustainable Energy*, vol. 6, no 2, pp. 635-643, Mar. 2015.
[7] Y. Ju, W. Wu, B. Zhang *et al*., "An extension of FBS three-phase power flow for handling PV nodes in active distribution networks," *IEEE Transactions on Smart Grid*, vol. 5, no. 4, pp. 1547-1555, Jul. 2014.
[8] S. Wang, L. Han, and L. Wu, "Uncertainty tracing of distributed generations via complex affine arithmetic based unbalanced three-phase power flow," *IEEE Transactions on Power Systems*, vol. 30, no. 6, pp. 3053-3062, Nov. 2015.
[9] I. Dzafic, B. C. Pal, M. Gilles *et al*., "Generalized π Fortescue equivalent admittance matrix approach to power flow solution," *IEEE Transactions on Power Systems*, vol. 29, no. 1, pp. 193-202, Jan. 2014.
[10] U. Ghatak and V. Mukherjee, "A fast and efficient load flow technique for unbalanced distribution system," *International Journal of Electrical Power & Energy Systems*, vol. 84, pp. 99-110, Jan. 2017.
[11] J. Csatár and A. Dán, "Novel load flow method for networks with multipoint-grounded-neutral and phase-to-neutral connected equipment," *International Journal of Electrical Power & Energy Systems*, vol. 107, pp. 726-734, May 2019.
[12] A. J. Urquhart and M. Thomson, "Series impedance of distribution cables with sector-shaped conductors," *IET Generation, Transmission & Distribution*, vol. 9, no. 16, pp. 2679-2685, Sept. 2015.
[13] H. Keshtkar, S. K. Solanki, and J. M. Solanki, "Improving the accuracy of impedance calculation for distribution power system," *IEEE Transactions on Power Delivery*, vol. 29, no. 2, pp. 570-579, Apr. 2014.
[14] F. Camilo, R. Castro, M.E. Almeida *et al*., "Self-consumption and storage as a way to facilitate the integration of renewable energy in low voltage distribution networks," *IET Generation, Transmission & Distribution*, vol. 10, no. 7, pp. 1741-1748, May 2016.
[15] W. H. Kersting, "Radial distribution test feeders," *IEEE Transactions on Power Systems*, vol. 6, no. 3, pp. 975-985, Aug. 1991.
[16] W. H. Kersting, "Radial distribution test feeders," in *Proceedings of IEEE PES Winter Meeting (Cat. No. 01CH37194)*, Columbus, USA, Feb. 2001, pp. 908-912.
[17] S. M. Moghaddas-Tafreshi and E. Mashhour, "Distributed generation modeling for power flow studies and a three-phase unbalanced power flow solution for radial distribution systems considering distributed generation," *Electric Power Systems Research*, vol. 79, no. 4, pp. 680-686, Apr. 2009.
[18] D. Rajičić and R. Taleski, "Two novel methods for radial and weakly meshed network analysis," *Electric Power Systems Research*, vol. 48, no. 2, pp. 79-87, Dec. 1988.
[19] C. Lin, Y. Huang, and C. Huang, "Distribution system load flow calculation with microcomputer implementation," *Electric Power Systems Research*, vol. 13, no. 2, pp. 139-145, Oct. 1987.
[20] B. Muruganantham, R. Gnanadass, and N. P. Padhy, "Performance analysis and comparison of load flow methods in a practical distribution system," in *Proceedings of 2016 National Power Systems Conference*, Bhubaneswar, India, Dec. 2016, pp. 1-6.
[21] E. Bompard, E. Carpaneto, G. Chicco *et al*., "Convergence of the backward/forward sweep method for the load-flow analysis of radial distribution systems," *International Journal of Electrical Power & Energy Systems*, vol. 22, no. 7, pp. 521-530, Oct. 2000.
[22] G. Luo and A. Semlyen, "Efficient load flow for large weakly meshed networks," *IEEE Transactions on Power Systems*, vol. 5, no. 4, pp. 1309-1316, Nov. 1990.
[23] M. Pais, M. E. Almeida, and R. Castro, "Voltage regulation in low voltage distribution networks with embedded photovoltaic microgeneration," in *Proceedings of International Conference on Renewable Energies and Power Quality (ICREPQ'12)*, Santiago de Compostela, Spain, Mar. 2012, pp. 503-508.
[24] J. L. Choque, D. Rodas, and A. Padilha-Feltrin, "Distribution transformer modeling for application in three-phase power flow algorithm," *IEEE Latin America Transactions*, vol. 7, no. 2, pp. 196-202, Jun. 2009.
[25] R. M. Ciric, A. Padilha Feltrin, and L. F. Ochoa, "Power flow in four-wire distribution networks – general approach," *IEEE Transactions on Power Systems*, vol. 18, no. 4, pp. 1283-1290, Nov. 2003.
[26] C. Cheng and D. Shirmohammadi, "A three-phase power flow method for real-time distribution system analysis," *IEEE Transactions on Power Systems*, vol. 10, no. 2, pp. 671-679, May 1995.
[27] K. Yamashita, S. Djokic, J. Matevosyan *et al*., "Modelling and aggregation of loads in flexible power networks – scope and status of the work of CIGRE WG C4.605," *IFAC Proceedings Volumes*, vol. 45, no. 21, pp. 405-410, Sept. 2012.
[28] A. Mahmoud and R. Shultz, "A method for analyzing harmonic distribution in A.C. power systems," *IEEE Transactions on Power Apparatus and Systems*, vol. PAS-101, no. 6, pp. 1815-1824, Jun. 1982.
[29] I. Archundia-Aranda and R. O. Mota-Palomino, "Harmonic load flow method for radial distribution networks," in *Proceedings of 14th International Conference on Harmonics and Quality of Power – ICHQP 2010*, Bergamo, Italy, Sept. 2010, pp. 1-5.
[30] R. Burch, G. Chang, C. Hatziadoniu *et al*., "Impact of aggregate linear load modeling on harmonic analysis: a comparison of common practice and analytical models," *IEEE Transactions on Power Delivery*, vol. 18, no. 2, pp. 625-630, Apr. 2003.
[31] G. W. Chang, P. F. Ribeiro, and S. J. Ranade, "Harmonics theory," in *Tutorial on Harmonics Modeling and Simulation*, Technical Report No. TP-125-0:8, Aug. 1998.
[32] F. M. Camilo, V. F. Pires, R. Castro *et al*., "The impact of harmonics compensation ancillary services of photovoltaic microgeneration in low voltage distribution networks," *Sustainable Cities and Society*, vol. 39, pp. 449-458, May 2018.
[33] S. Hardie and N. Watson, "Power quality implications of new residential appliances," in *Proceedings of Electricity Engineers' Association (EEA) Annual Conference*, Christchurch, New Zealand, Jun. 2010, pp. 1-6.
[34] J. Niitsoo, I. Palu, J. Kilter *et al*., "Residential load harmonics in distribution grid," in *Proccedings of 3rd International Conference on Electric Power and Energy Conversion Systems* (EPECS 2013), Istanbul, Turkey, Oct. 2013, pp. 1-6.
[35] A. Nassif, "Modeling, measurement and mitigation of power system harmonics," Ph.D. dissertation, University of Alberta, Edmonton, Canada, 2010.
[36] L. Schwartfeger, D. Santos-Martin, A. Wood *et al*., "Review of distributed generation interconnection standards," in *Proceedings of Electricity Engineers' Association Conference*, Auckland, New Zealand, Jun. 2014, pp 18-20.
[37] A. Chidurala, T. Saha, and N. Mithulananthan, "Harmonic characterization of grid connected PV systems & validation with field measurements," in *Proceedings of IEEE PES General Meeting*, Denver, USA, Jul. 2015, pp. 1-5.
[38] D. Pileggi, N. Chandra, and A. Emanuel, "Prediction of harmonic voltages in distribution systems," *IEEE Transactions on Power Apparatus and Systems*, vol. PAS-100, no. 3, pp. 1307-1315, Mar. 1981.
[39] I. Archundia-Aranda and R. O. Mota-Palomino, "Harmonic penetration method for radial distribution networks," *International Journal of Emerging Electric Power Systems*, vol. 15, no. 2, pp. 111-117, Apr. 2014.
[40] Y. Liu, M. Marz, T. Ortmeyer *et al*., "Test systems for harmonics modeling and simulation," *IEEE Transactions on Power Delivery*, vol. 14, no. 2, pp. 579-587, Apr. 1999.
[41] W. M. Grady and R. J. Gilleskie, "Harmonics and how they relate to power factor," in *Proceedings of EPRI Power Quality Issues & Opportunities Conference (PQA'93)*, San Diego, USA, Nov. 1993, pp. 1-8.
[42] J. C. Das, *Power System Harmonics and Passive Filter Designs*, Hoboken: John Wiley & Sons, 2015.
[43] A. Almeida and P. Fonseca. (2008, Jan.). Residential monitoring to decrease energy use and carbon emissions in Europe. [Online]. Available: https://www.researchgate.net/publication/228616014
[44] *Conductors of Insulated Cables*, British Standard EN 60228, 2015.
[45] Energy Services National Regulatory Authority, "Consumption profiles and microgeneration three-phase radial distribution systems for 2018," Portugal Technical Report, 2018.
[46] *Voltage Characteristics of Electricity Supplied by Public Distribution System*, British Standard EN 50160, 2000.
[47] C. Y. Lee, "Effects of unbalanced voltage on the operation performance of a three-phase induction motor," *IEEE Transactions on Energy Conversion*, vol. 14, no. 2, pp. 202-208, Jun. 1999.
[48] *Effects on Unbalanced Voltages on the Performance of Induction Motors*, IEC Standard 60034-26, 2002.

Fernando M. Camilo received the Ph.D. degree in electrical and computer engineering from Técnico Lisboa, University of Lisbon, Lisbon, Portugal, in 2020. He is a Junior Researcher at Instituto de Engenharia de Sistemas e Computadores, Investigação e Desenvolvimento (INESC-ID), Lisbon, Portugal. His research has resulted in several publications in top international journals. His research interests include power systems, storage systems, photovoltaic energy, and renewable energy.

M. E. Almeida received the Ph.D. degree in electrical and computer engineering from Técnico Lisboa, University of Lisbon, Lisbon, Portugal, in

1999. She is currently an Assistant Professor at Técnico Lisboa, and a Researcher at Instituto de Engenharia de Sistemas e Computadores, Investigação e Desenvolvimento (INESC-ID), Lisbon, Portugal. Her main research interests include line modelling, high-voltage engineering, and electromagnetic transients.

Rui Castro received the Ph.D. degree in electrical and computer engineering from Técnico Lisboa, University of Lisbon, Lisbon, Portugal, in 1994. He is currently working as an Associate Professor at Técnico Lisboa, and as a Senior Researcher at Instituto de Engenharia de Sistemas e Computadores, Investigação e Desenvolvimento (INESC-ID), Lisbon, Portugal. He is the author of two books and more than 100 articles in journals and international conferences. His research interests include renewable energy, storage systems, electricity markets, and power systems.

V. Fernão Pires received the Ph.D. degree in electrical and computer engineering from Técnico Lisboa, University of Lisbon, Lisbon, Portugal, in 2000. Since 1991, he is a member of the teaching staff at the Electrical Engineering Department of Superior Technical School of Setúbal - Polytechnic Institute of Setúbal, Setúbal, Portugal. Presently, he is a Professor teaching Power Electronics and Control of Power Converters. He is also a Researcher at Instituto de Engenharia de Sistemas e Computadores, Investigação e Desenvolvimento (INESC-ID). His work has resulted in more than 200 publications in journals and conferences. His present research interests include renewable energy, electrical vehicles, storage systems, and power quality.